Annual Report for

A Study of the Relationship Between Macroscopic Measures and Physical Processes Occuring during

N0014-89-J-1708

submitted to:

Office of Naval Research
Attn. Dr. George Yoder
ONR Code 1131
800 N. Quincy
Arlington, Virginia 22217-5000

by

Stephen D. Antolovich
Mechanical Properties Research Lab
School of Materials Engineering
Georgia Institute of Technology
Atlanta, GA 30332-0245

Stuart R. Stock
Mechanical Properties Research Lab
School of Materials Engineering
Georgia Institute of Technology
Atlanta, GA 30332-0245

TABLE OF CONTENTS

TABLE OF CONTENTS - CONTINUED

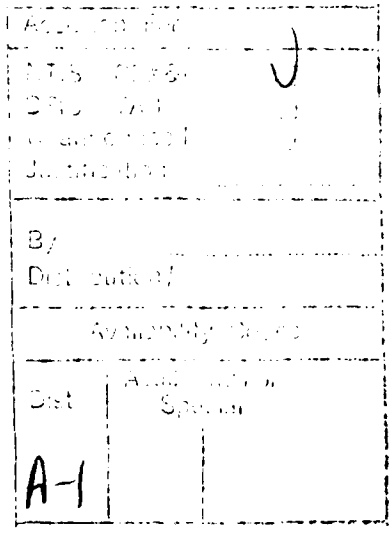

I. Physical Measurements of Crack Closure

A. Accomplishments during the past year

The principal experimental accomplishments during the second year of the program were two sets of x-ray tomographic microscopy (XTM) measurements on notched tensile samples. Fatigue crack growth was in a conventional servo-hydraulic machine before the samples were mounted in the in situ load frame. The particulars for crack growth were: R=0.1 and 5 Hz haversine waveform. Some alteration of the maximum load was used; these details are outlined in the technical publications. Once the samples were gripped in place in the minature load frame (pictured with the CCD x-ray camera in Fig. 1), the sample was loaded to the maximum level (a load equal to or slightly less than that used to propagate the crack, depending on whether the crack was propagating stably at the end of crack growth in the servo-hydraulic apparatus) and was allowed to equilibrate mechanically. The first set of projections were then recorded. The load was decremented by a pre-determined fraction of the maximum load for that sample, and another set of projections was recorded. This progression was repeated until data for reconstructions was obtained for all desired loads. Reconstruction of slices of the sample followed the end of the experiments and was with the filtered back projection method.

The choice of the extremely small (by fracture mechanics standards) samples was dictated by the need to have good sample transparency at the synchrotron x-ray energies with the highest fluxes (typically up to about 25 keV before the flux starts to drop dramatically). A second consideration limiting the sample diameter is the number of detector elements and the maximum cross-sectional dimension of the sample: a 10 mm diameter sample sampled with 10^3 detector elements yield a minimum pixel dimension of 10 μm; closure measurement requires pixels smaller than this. An unanticipated advantage of the smaller sample size is that the load-displacement record shows features which are normally not present in traces of larger samples. Presumably this is due to more "averaging" in larger samples. The enhanced sensitivity will be very interesting to interpret. As is noted in the future work section, XTM should be able to obtain similar resolution images in both large (10 mm maximum diameter) and small (2 mm diameter) samples if region-of-interest (ROI) sampling techniques are used whereas the sensitivity of stiffness measurements cannot be preserved.

The first notched tensile sample examined with XTM (NT-3) had an initial diameter of 2.09 mm, and at the end of the test (after 61850 cycles) the crack had decreased the effective load-carrying cross-section of the sample to 1.85 mm (as measured by the change in compliance of the sample). The original plan was to collect data at Stanford Synchrotron Radiation Laboratory (SSRL) in April 1990 using beamtime assigned to our collaborators at Lawrence Livermore National Laboratory (LLNL); the Georgia Tech proposal for crack closure

measurements, however, was not yet eligible for beamtime. Some very curious choices were made by those responsible at LLNL for assigning their portion of beamtime on beamline X; no time was given to our collaborators at LLNL despite their strong record of scientific accomplishment and the fact that they were the only LLNL group (using synchrotron radiation) to obtain external funding for their research. Instead of running at SSRL, the XTM experiments were performed at Dr. J.H. Kinney's laboratory at LLNL using a standard sealed tube x-ray source.

The experiments at LLNL were very successful. The x-ray source was an Ag tube with effective spot size of 1 x 1 mm^2 (producing penumbral blurring of about 13 μm at the CCD detector-- compared to essentially no penumbral blurring for synchrotron radiation experiments) and was operated at 40 kV and 30 mA. One sample was characterized during the experiment; loads of 81.7, 50.0, 25.0, 4.5 and 0 kg (95, 58, 29, 5 and 0 %, respectively, of the maximum load under which the crack propagated) were studied. The 2.9 mm diameter slice, shown in Fig. 2, was reconstructed with 6.2 μm pixels using 1 deg angular increments between views. Note that the slice was from just above the center of the notch and that the data was obtained at an applied load of 81.7 kg. The nonplanar fatigue crack was also clearly visible in many of the other simultaneously recorded slices.

It was found that a better way to visualize the three-dimensional crack (short of volume rendering!) was to use "cuts" parallel to the load axis instead of slices perpendicular to the load axis. The cuts shown in Fig. 2b-2d were obtained for 81.7, 50.0 and 25.0 kg loads; the scales throughout Fig. 2 were chosen to be identical. The same volume of material was sampled in the 6.2 μm thick cuts. Changes in crack opening were quite pronounced, and parts of the crack disappeared at low applied loads. Comparison of the cuts with a digital radiograph were quite revealing: even at high load the crack was invisible in radiographs (i.e. individual views) but the computed tomography reconstruction process allowed the volume of material outside of the cut of interest to be stripped away.

The fatigue crack in a second notched tensile sample (NT-4) was characterized at Cornell High Energy Synchrotron Source (CHESS) during September 1990. The sample's initial diameter was 1.89 mm, and the effective decrease in sample cross-section was 110 μm after 34,760 cycles. The testing parameters were the same as given above. The object in stopping the crack growth at a relatively short length was to test the sensitivity of XTM to the smallest range of crack openings one would be likely to encounter and to allow the crack to be grown further for additional XTM characterization. Looking at the same crack before and after it extends should allow ellucidation of the role of near-crack-tip closure and of contact "far" from the crack tip: the crack face positions near the crack tip in the first measurement could be compared, as a function of load, with the same faces, now far removed from crack tip, in the second measurement.

The XTM experiments at CHESS were also extremely successful and showed the ability of the GT/LLNL/Sandia team to perform the in situ XTM loading experiments in a routine fashion (at least of notched tensile samples!). The x-ray energy used to record the data was 22 keV, 1 deg angular increments were used between views and the sample volume containing the crack was reconstructed with 5.6 μm x 5.6 μm x 5.6 μm voxels. Ten load levels were studied: 45.5, 36.4, 27.0, 18.2 and 9.1 kg (100, 80, 60, 40 and 20 %, respectively, of the maximum load during the fatigue cycles preceeding the interuption of the test) on an unloading cycle and 40.9, 31.8, 22.7, 13.6 and 4.6 kg (90, 70, 50, 30 and 10 %, respectively, of the maximum load) on the next unloading cycle. Figure 3 shows a typical 1.9 mm slice under 45.5 kg load and three 5.6 μm thick cuts parallel to the load axis and through the same volume of material at 45.5 kg, 27.0 kg and 9.1 kg loads. In these cuts the crack is much less pronounced than in those of sample NT-3 which is expected because the crack in NT-4 is much shorter. It also is clear that the images are much sharper in the synchrotron data; this difference should persist, albeit much less prominently, even when a microfocus source (down to a 10 μm diameter spot size) is used to eliminate penumbural blurring in laboratory measurements.

Detailed analysis of the CHESS data is currently in progress. Crack opening in a given slice of the sample was the initial method used to quantify closure as a function of applied load. This simple approach appeared to be inadequate; large scatter in the opening measured in this fashion was superimposed on the overall decreasing crack width (for the corresponding pixel in different slices) as the load decreased. As the crack is at a significant angle to the slices (i.e. the crack's intersection with the slice was never planar), measuring changes in crack width in the plane of the slices would be particularly insensitive. A much more sensitive means of quantifying crack closure is to measure the crack opening in cuts parallel to the load axis; one can also easily focus on the tips of asperities and on the "peaks" and "valleys" of the zig-zag crack by using cuts. This work has begun, and the approach to be taken is described in the following section. One should note that one could also use the change in separation <u>normal</u> to the local crack faces as the measure of closure; plans for this type of analysis are described in the following section.

B. Difficulties Encountered

Some difficulties which could not have been anticipated have been encountered during the past year. One was the difficulty obtaining beam time during SSRL's Spring 1990 run; this was described above. A benefit was that the laboratory XTM experiments on sample NT-3, the first for the in situ load frame (the first ever in situ loading during XTM), were conducted without the pressure of using every minute of beam time. Relatively minor problems (e.g. rubbing of the CCD detector faceplate and the stage's stand-off tube) were

ironed out without significant impact on the amount of data collected. The usefulness of laboratory XTM with the LLNL apparatus was clearly demonstrated; these results, even with the large penumbral blurring (which can be eliminated if a commonly available microfocus source is used), demonstrate that **XTM is a powerful technique for studying in situ materials processes--** a technique **which can be included in any laboratory.** The capital cost of the LLNL apparatus and a suitable x-ray generator are below those of a good SEM; the workstations required for apparatus control and data acquisition are relatively inexpensive, with prices rapidly decreasing. It should be possible to license the LLNL software if organizations wish to obtain first-rate XTM capabilities rapidly.

The second, more serious difficulty encountered was the need for considerably greater computing power and hard drive memory. The capabilities of the Micro VAX-II on which reconstructions have been performed and data analysis is done have been exceeded. Reconstruction of each slice requires about 45 minutes if this program is the only one being executed; current medium performance workstations require about 10 min per slice and a 40-processor SPRINT unit requires less than 0.5 min per slice. Also, the Micro VAX-II is required to operate in a multi-user mode, and some of the other users run fairly elaborate finite element programs. The competition tends to slow data analysis. A third area of concern is the availability of only 600 MBytes of storage for XTM data on the Micro VAX-II. This small size can be put in perspective by the following. The September run at CHESS brought back about **8 GBytes** of data on 8 mm tape, and a typical sample (e.g. a single load level in the present instance) occupies about 60 MBytes. If all ten loads recorded for NT-4 were on the hard drive at one time, no other work could proceed. One should note using supercomputers would require writing a considerable amount of code and would not address our data storage difficulties.

Contingency for upgrading computing capabilities was budgeted, and expenditure of these funds should improve the rate at which the closure data can be analyzed. Considerable leverage has been obtained with other funded programs. First, the School of Materials Engineering has designated two SUN workstations for use in XTM. These will be used for the most intensive numerical calculations (e.g. back projection) which will free the other computers for data analysis. A 1.2 GByte hard drive will be added to the SUNs. A second 1.2 GByte drive will be added to a DEC 3100 workstation (in the Georgia Tech Research Institute) which will also be available for XTM. Once these additions have been implemented, the bottleneck in processing the data should be reduced considerably.

II. Analytical Computations of the Effective Stress Intensity Factors

A. Rigid and Elastic Asperities in an Elastic Medium

In the previous report, some basic expressions for calculating the effective stress intensity factor for simple cases using a rigid cylinder were developed. In the present report, more realistic models for crack closure are analyzed by considering an asperity of an arbitrary shape which relates to different grain sizes and orientations. The width and the location of the asperity are parameterized. The same procedure as in the previous work is followed to obtain the effective stress intensity factor for rigid and elastic asperities between two crack surfaces. The appropriate models are shown in Figs. 4 and 5. The loading scheme and important quantities for crack closure are shown in Fig 6.

Considering the crack opening displacements due to the remote stress, σ, and the contact internal pressure, p', and the deformation of the asperity, the closure stress intensity factor in terms of asperity parameters and crack opening load, σ_{op} is as follows:

Case 1 $\quad \sigma_{op} \geq \sigma_{cl} \geq -\left[\frac{C_i}{1-C_i}\right]\sigma_{op}$

$$\frac{Ki}{\sigma_{op}\sqrt{\pi a}} = Ci + (1-Ci)\frac{\sigma_{cl}}{\sigma_{op}} \qquad \ldots(1)$$

(i=0, 1 for rigid and elastic cases respectively). C_0 and C_1 depend only on asperity properties. They are given by:

$$C_0 = \frac{G'}{H} \qquad \ldots(2)$$

and

$$C_1 = \frac{G'}{H + \frac{1}{4}\left(\frac{w}{a}\right)\frac{1}{F}\alpha\pi} \qquad \ldots(3)$$

Here, G', H and F are given as influence functions in the calculation of the stress intensity factor considering crack opening displacement for external and internal loads. The second term in the denominator of C_1 involving the asperity shape factor, α, accounts for elastic deformation of an asperity.

Case 2

(b) $\sigma_{cl} \leq -[\frac{C_i}{1-C_i}]\sigma_{op}$

$$K_i = 0 \qquad (i=0,1) \qquad \ldots(4)$$

Equations (1) and (4) are shown schematically in Fig. 7. The contact pressure between the crack surface and the asperity, Fig. 8, is calculated from:

$$P_i' = \frac{\pi C_i}{G'}(\sigma_{op} - \sigma_{cl}) \qquad (i=0,1) \qquad \ldots(5)$$

Using the above results, the effective stress intensity factor is:

$$\begin{aligned}\Delta K &= K_{max} - K_{cl} \\ &= [1 - C_i\frac{\sigma_{op}}{\sigma_{max}} - (1-Ci)\frac{\sigma_{cl}}{\sigma_{max}}]\sigma_{max}\sqrt{\pi a} \qquad (i=0,1)\end{aligned} \qquad (6)$$

When $\sigma_{cl} = \sigma_{op}$, there is no closure effect and ΔK is given by simply $(\sigma_{max} - \sigma_{op})\sqrt{\pi a}$. However, when $\sigma_{cl} = 0$, there is a factor of C_i in the opening stress, σ_{op}, i.e.

$$\Delta K = (\sigma_{max} - C_i\sigma_{op})\sqrt{\pi a} \qquad (i=0,1) \qquad \ldots(7)$$

B. Correction of the Stress Intensity Parameter Due to the Crack Tip Plastic Zone

Irwin's plastic zone correction model may be used for the correction of the stress intensity parameter if the strength of the singularity at the crack tip is considered to be primarily affected by plastic deformation. Then, in all previous expressions, a and c must be replaced by $a' = a + r_p^*$ and $c' = c + r_p^*$, respectively. Here, r_p^* is $\frac{a}{6}(\frac{\sigma}{\sigma_{yp}})^2$

III. Finite Element Analysis for Computation of Stress Intensity Parameters

A center-cracked thick plate with remote stresses (Fig. 9) was used as a model for calculating stress intensity parameters. Due to symmetry, only the upper half of the specimen (Fig. 10) was discretized by using a total of 457 and 490 quadratic, isoparametric elements as shown in Figs. 11 and 12. A two step loading scheme composed of increasing and decreasing loads (Fig. 6) was adopted to study crack closure behavior. Crack closure for the rigid asperity was modelled by simply holding any points at which the asperity was located when the applied stress reached the opening stress, σ_{op}, and by decreasing the load until it reached any closure loads, σ_{cl}. In this study σ_{cl} was considered zero, so that the stress in the specimen body was fully relaxed. Crack closure for the elastic asperity was modelled by adding one or a few more elements at the position of the asperity on the crack surface and by holding the bottom side of additional elements in place when the element reached the specimen symmetric line during the decreasing loading process. This involved significant complexity in monitoring the displacement of the nodes of additional elements and determining the load which gave the predicted displacements. An incremental finite element approach was taken to adapt the two step loading scheme to numerical analysis. Node holding processes were performed by changing boundary conditions, i.e., from free to fixed boundary condition. (A secondary way of holding the node by assigning very large stiffness to the nodes was abandoned because of convergence problems.) The strain energy release rate method and J-integral method were used as solution techniques to find the stress intensity parameter. As seen in the previous report, the strain energy release rate method proved to be superior in solving the problem involving contact near the crack tip.

IV. Results and Discussion of Analytical Studies

Figs. 13 and 14 show variations of the closure stress intensity factors obtained from analytical computations for both rigid and elastic asperities. In Fig. 13, it is shown as a function of position for a given asperity width. In Fig. 14, it is shown in terms of width for a given asperity location. From Fig. 13, it is seen that there is not much difference in the stress intensity factor for rigid or elastic asperities. However, there are significant differences as the width changes, Fig. 14. In both cases, the closure stress intensity factors increase as the asperity approaches the crack tip, which is physically reasonable, since it is near the crack tip that the stress distribution would be most perturbed.

The same comparisons for contact pressure obtained from analytical work are made in Figs. 15 and 16. In these figures, the values of pressure are normalized by the difference between the opening and closure load. At a given asperity location, the pressure is higher for rigid material, as expected. In Figure 16, it is

important to note that the contact pressure drops rapidly for small increases in asperity width.

In Figs. 17, 18 and 19, finite element results confirm the correctness of the analytical work. As seen as in the previous report, the J-integral technique gives erroneous results near the crack tip, as evidenced by divergence from the analytical solutions. This can be understood in terms of a shrinking K-dominated zone when asperity contact is near the crack tip. Consequently, it is very difficult to model the crack tip behavior when J-integral approaches are used.

V. Plans for the Third Year of the Program

A. Closure Measurements

Activity during the coming year will cover many areas.

1. FCP Experiemnts

Fatigue crack propagation will be performed with the small compact tension samples. These experiments will determine whether or not testing procedures and sample size produce appreciable differences in crack propagation rates from those observed in earlier work. Initial indications are that we have excellent correspondence with the earlier work. If close agreement is found, interpretation of the XTM results and stiffness measurements on the much smaller samples will be considerably simplified. Conversely, if the crack growth rates differ due to an unanticipated size effect, this will indicate a more cautious extrapolation of XTM results to full-sized compact tension samples.

2. Closure in Notched Tensile Samples

Analysis of the physical closure process will continue for the notched tensile samples NT-3 and NT-4. Work will continue on crack face separations measured in cuts parallel to the load axis. Work will also begin on volume rendering of the three-dimensional data; this coupled with direct subtraction of volumes should provide superior visualization of the locations where significant crack face contact is occurring. The imaging language used by our group (IDL) should allow this to be done relatively efficiently.

3. Synchrotron XTM of NT-4 after Crack Extension

Synchrotron XTM will be carried out on sample NT-4 after crack extention. As discussed above, this would allow assessment of the relative contributions of near-tip and far-from-the-tip crack face interactions to the macroscopically observed closure. Whether or not this can be accomplished depends on whether the

crack can be extended without fracturing the sample.

4. Region of Interest XTM of CT Specimens

Synchrotron XTM will be performed on a compact tension sample using Region-of-Interest sampling. The first sample to be characterized will have the some of the back surface removed so that data collection will be relatively straight-forward. The crack will be grown prior to removing material, and the crack length will be kept short relative to the remaining ligament. Methods are being investigated for assuring that the crack-tip in the reduced section sample is brought to the same state during in situ XTM load experiments as in the full width sample. It should be emphasized that the reduced ligament compact tension samples are primarily intended as an evolutionary step before examining a completely intact compact tension sample-- a sample which can be remounted in a servohydraulic apparatus for further crack extension and for which interpretation of results will be straight-forward.

5. Load Frame Modifications

While the first generation load frame has worked exceptionally well, the stand-off tube does have a slight effect on the images obtained: the path length of the x-rays through the tube varies somewhat from the edge of a view to its center. A preliminary design for a second generation load frame has been completed. The new design eliminates the stand-off tube. Further refinement will continue, but it is unlikely that the load frame will be built unless further funds are available from another source; this is being actively pursued.

6. Publications

A considerable number of publications and presentations at national meetings are planned.

B. Analytical Studies

1. Multiple Asperity Studies

To date we have had success in modelling single asperities. In the next phase of the study, we will model multiple asperities to more closely approach what occurs in reality.

2. Modelling of Idealized Fracture Surface

In this phase of the study, we will use stereological techniques to characterize the the fracture surface. The surface will then be represented in 2-dimensional, idealized form with the widths and heights of the asperities corresponding to the most salient measured features on the actual fracture surface. FCP specimens

that were mentioned in the preceeding section will be used for the surface characterization studies.

3. Use of XTM Results in Analytical/Numerical Models

The experimental XTM results that are obtained (i.e. geometry and loads at closure) will be fed into the analytical/numerical models for computation of forcing functions and for "normalization" of the FCP rates. The advantage to this approach is that the forcing functions will have an analytical basis and the details of the loads and fracture surfaces will correspond to what is measured in the bulk of the material.

4. Forcing Functions for Real Fracture Surfaces

The next level of complexity will be to computer model the actual fracture surface to obtain appropriate forcing functions for the material of interest.

5. Publication

We now have significant results and intend to present them at numerous mechanics/materials related conferences during the next year.

VI. Personnel

The following personnel have worked on the project

A. Principal Investigators

1.	Stephen D. Antolovich	Fracture Mechanics analytical studies, mechanical testing issues
2.	Stuart R. Stock	Tomography, radiography, specimen design, primary contacts with synchrotron sources, design of rig, mechanical testing issues

B. Students

1.	Thomas Breunig	Design of tensile rig, mechanical testing, tomography data acquisition
2.	Abbas Guvenilir	Assistance with design of experiments, analysis of data, tomography data acquisition

3. Y. Jung — Finite element calculations

VII. Interactions

Interaction with other groups is important to the success of the project. The following interactions have been (or are being) established:

	Organization	Person	Comments
1.	Lawrence Livermore	John Kinney	Active collaboration software, laboratory and synchrotron x-ray tomographic microscopy
2.	Southwest Research Institute	David Davidson	Continuing discussion on closure discussion
3.	CNAM (France)	C.Bathias	Discussions of closure in Al-Li alloys
4.	Stanford Synchrotron Radiation Laboratory	-	Proposal for beam time
5.	National Synchrotron Light Source		Proposal for beam time
6.	Cornell High Energy Synchrotron Source	-	Experiment performed

VIII. Presentations and Publications

1. (Invited) "X-Ray Tomographic Microscopy of Materials," American Crystallographic Association, 40th Annual Meeting, April, 1990, New Orleans.

2. "A Framework Relating Macroscopic Measures and Physical Processes of Crack Closure of Al-Li Alloy 2090" (presented by T.M. Breunig), 22nd National Symposium on Fracture Mechanics, June 1990, Atlanta.

3. "X-Ray Tomographic Microscopy of Materials", TMS-AIME Fall Meeting, 1990, Detroit, MI, October 1990.

4. "Nondestructive X-ray Tomographic Microscopy of Damage in

Metal Matrix Composites", ASTM International Symposium on Damage Defection and Quality Assurance in Composite Materials, November 1990, San Antonio.

5. "Impact of a SiC/Al MMC of X-ray Tomographic Microscopy on Deformation Studies," (presented by T.M. Breunig) Fall 1990 Materials Research Society Symposium on Advanced Tomographic Imaging Methods for the Analysis of Materials, November 1990, Boston.

Publication

"A Framework Relating Macroscopic Measures and Physical Processes of Crack Closure of Al-Li Alloy 2090," T.M. Breunig, S.R. Stock, S.D. Antolovich, J.H. Kinney, W.N. Massey and M.C. Nichols, to appear in 22nd National Symposium on Fracture Mechanics, 1990.

IX. Trade journals articles (written by the journal's staff) mentioning the in situ load frame and the XTM results.

Aerospace America, Feb. 1991, Designer's Notebook, pp.44-45.
Ceramic Bulletin, Feb. 1991, **70**, p. 203.
Metalworking News, June 18, 1990, pp. 6,20.

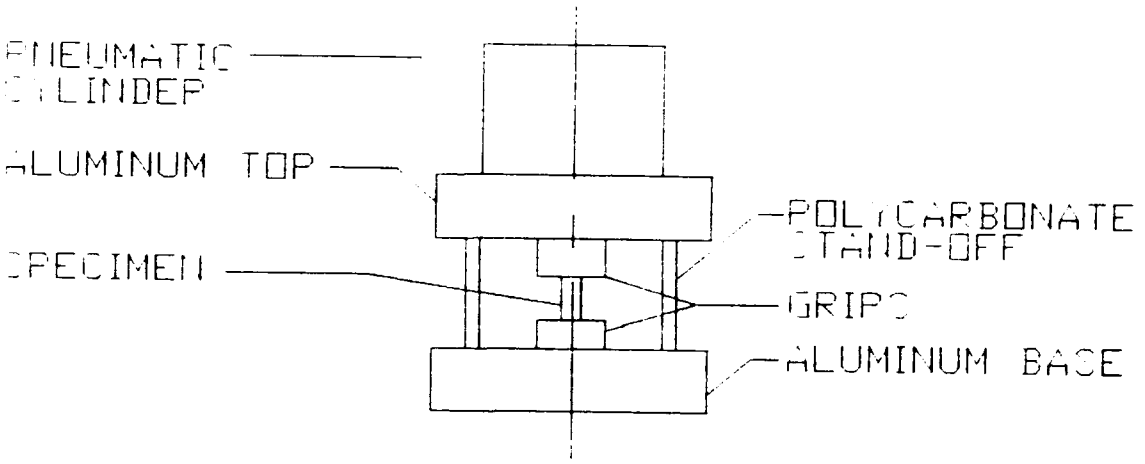

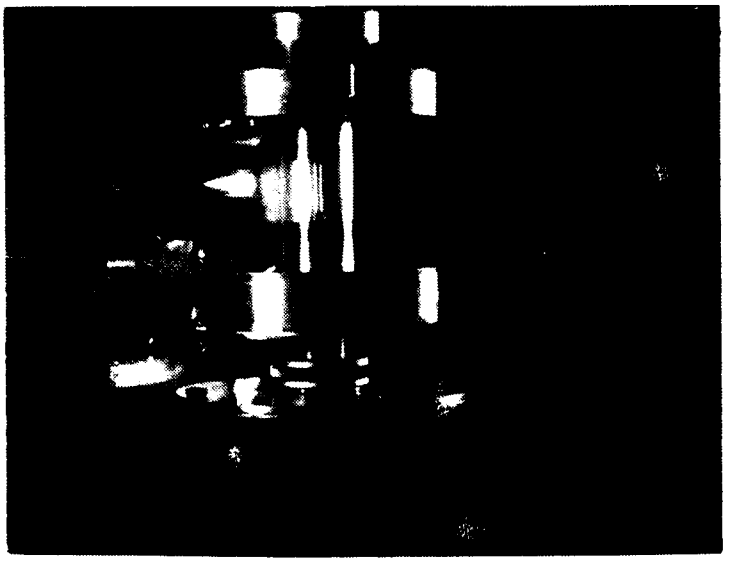

Figure 1. Schematic and photograph of the compact load frame for in situ AFM. The unique feature of this load frame is the polycarbonate stand-off supporting the applied load while allowing the sample to be viewed from all directions around the load axis.

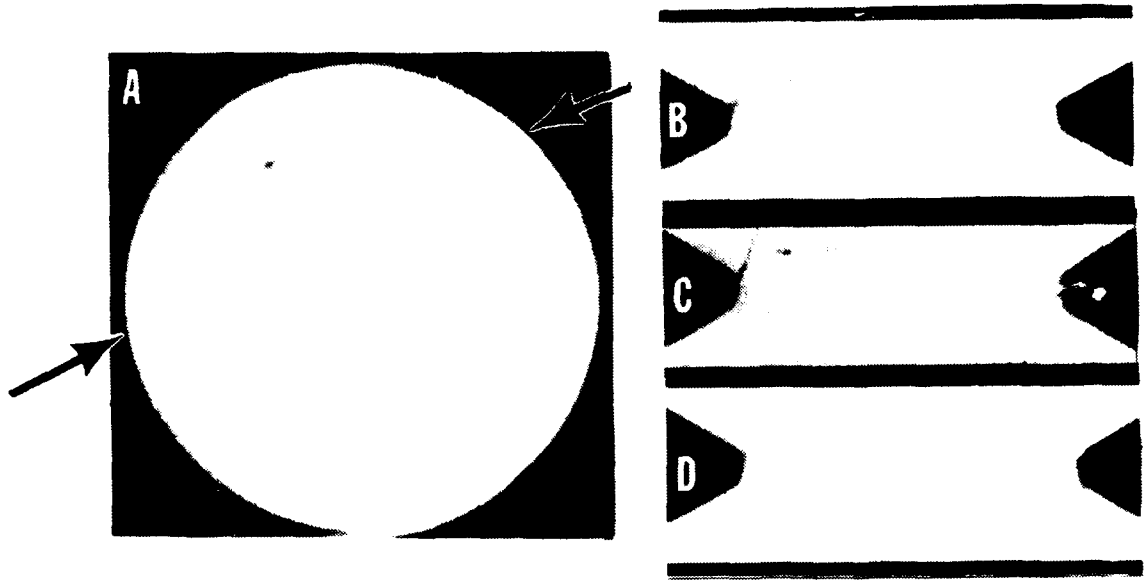

Figure 2. Laboratory XTM. a. Slice perpendicular to the load axis showing the fatigue crack darker than the matrix. The slice diameter is 2.9 mm, the applied load is 81.7 kg and the arrows show the location of the cuts. b.,c.,d. Cuts parallel to the load axis at loads of 81.7, 50.0 and 25.0 kg, respectively.

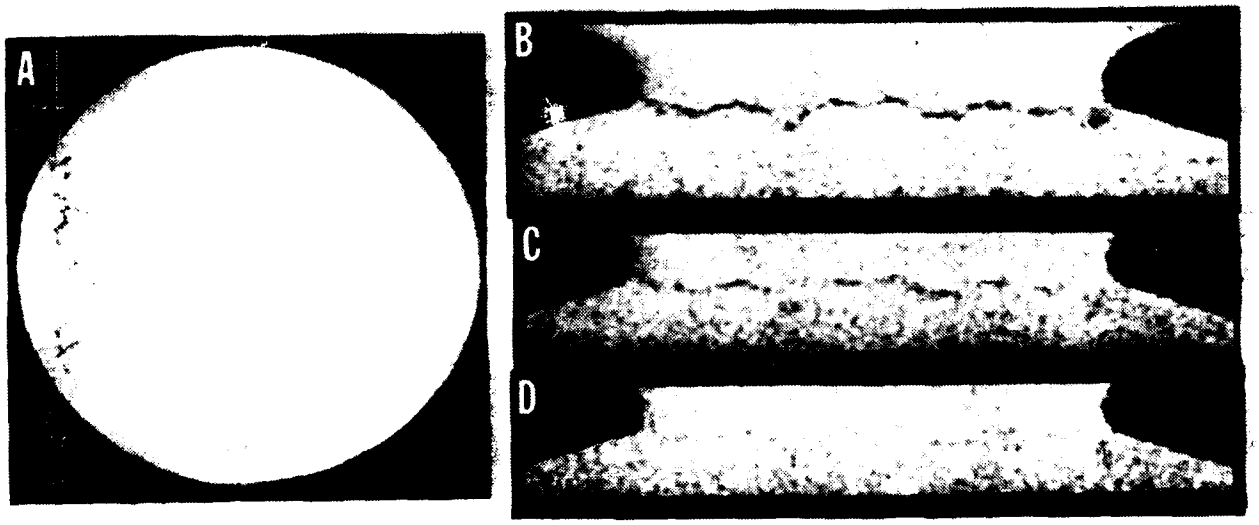

Figure 3. Synchrotron XTM. a. Slice perpendicular to the load axis showing the fatigue crack darker than the matrix. The sample diameter is 1.9 mm, the applied load is 45.5 kg and the arrows show the location of the cuts shown in b.- d. b.,c.,d. Cuts parallel to the load axis at loads of 45.5, 27.0 and 9.1 kg, respectively.

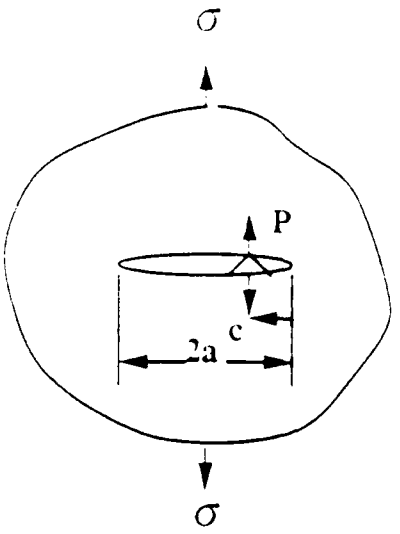

Fig. 4. Asperity in an infinite body

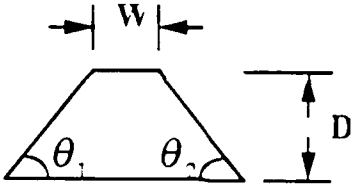

Fig. 5 Asperity Dimension

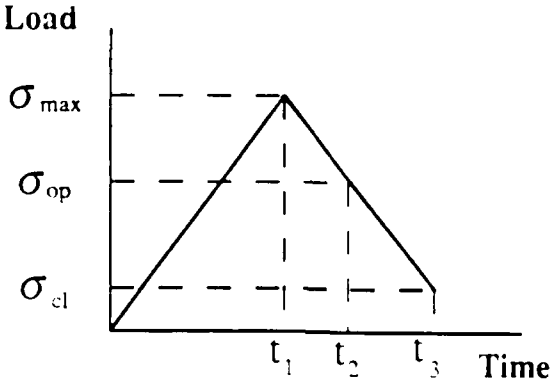

Fig. 6. Loading Scheme

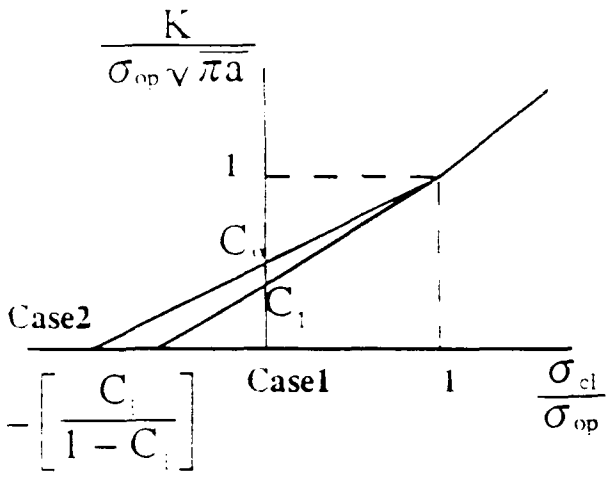

Fig 7. Graphical representation of K

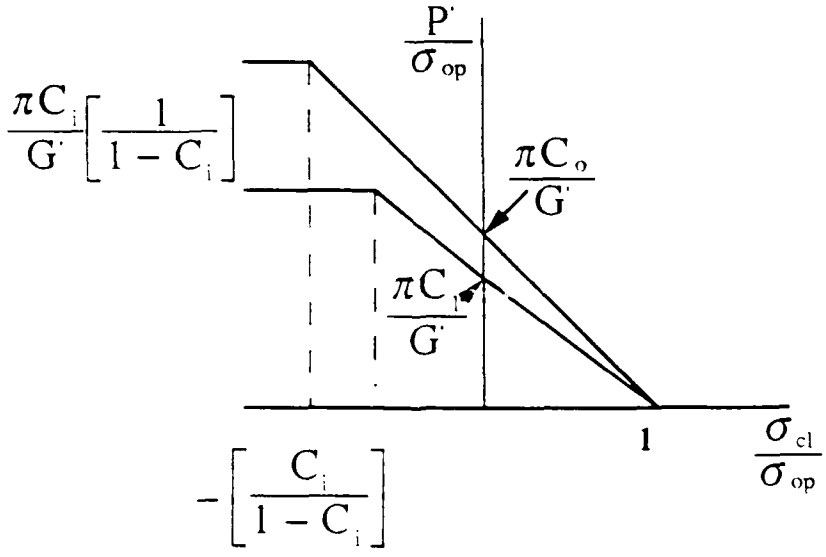

Fig. 8. P as a function of σ_{cl}/σ_{op}

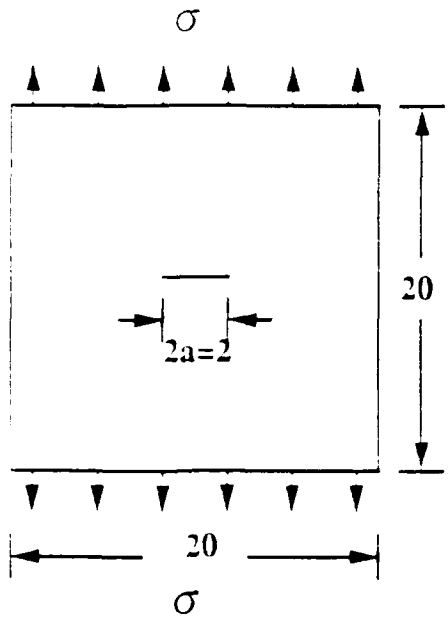

Fig. 9. Specimen Geometry

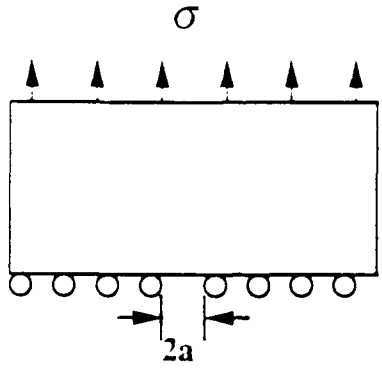

Fig. 10. Half Model

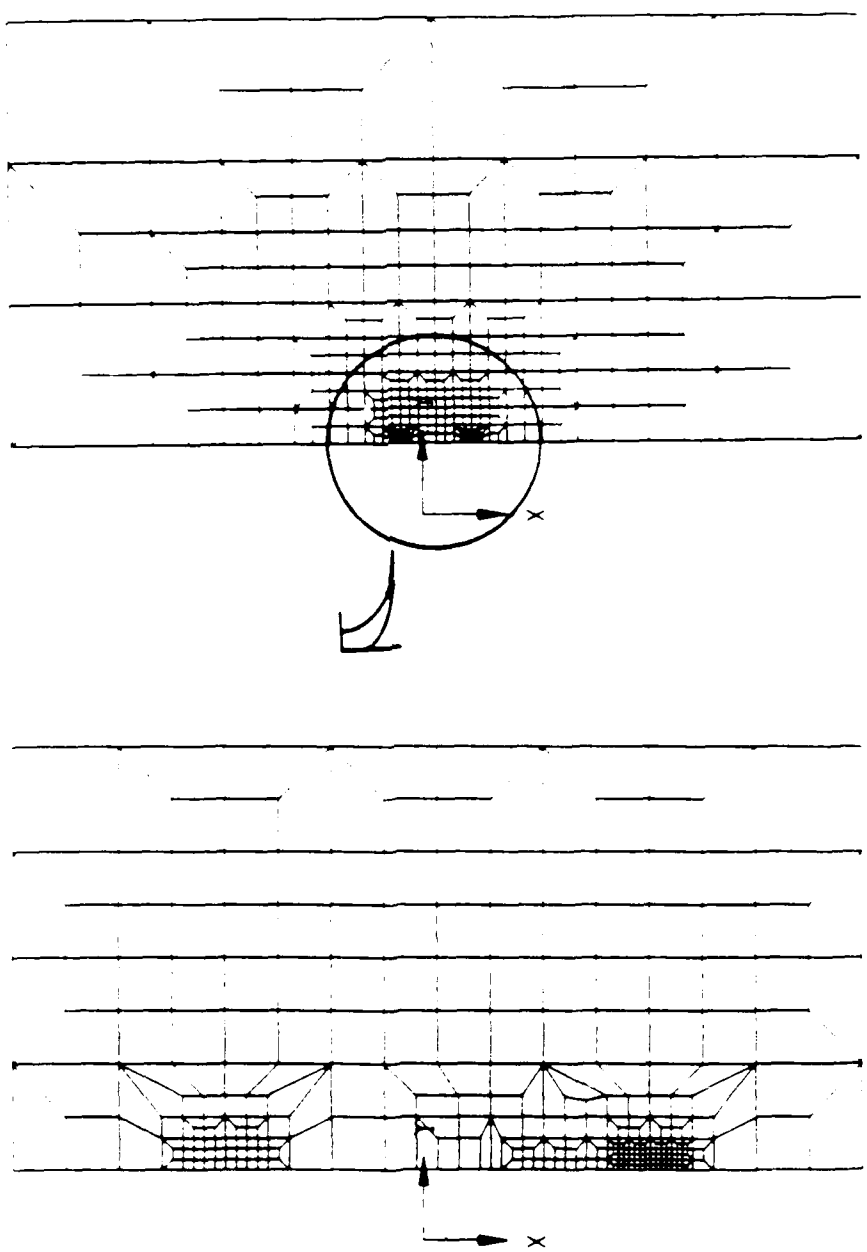

Fig. 11. Finite Element Mesh for a Rigid Asperity

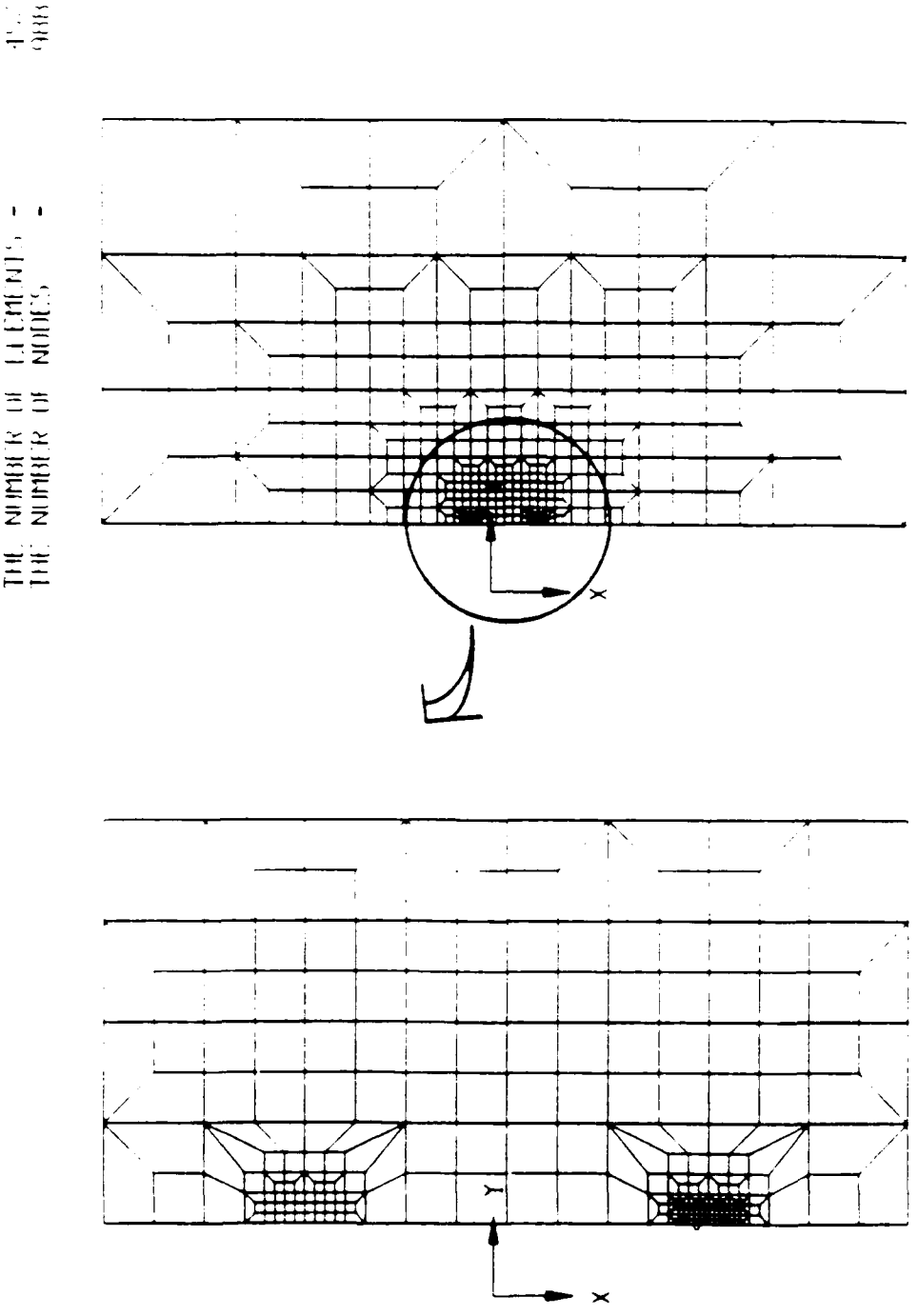

Fig. 12. **Finite Element Mesh for an Elastic Asperity**

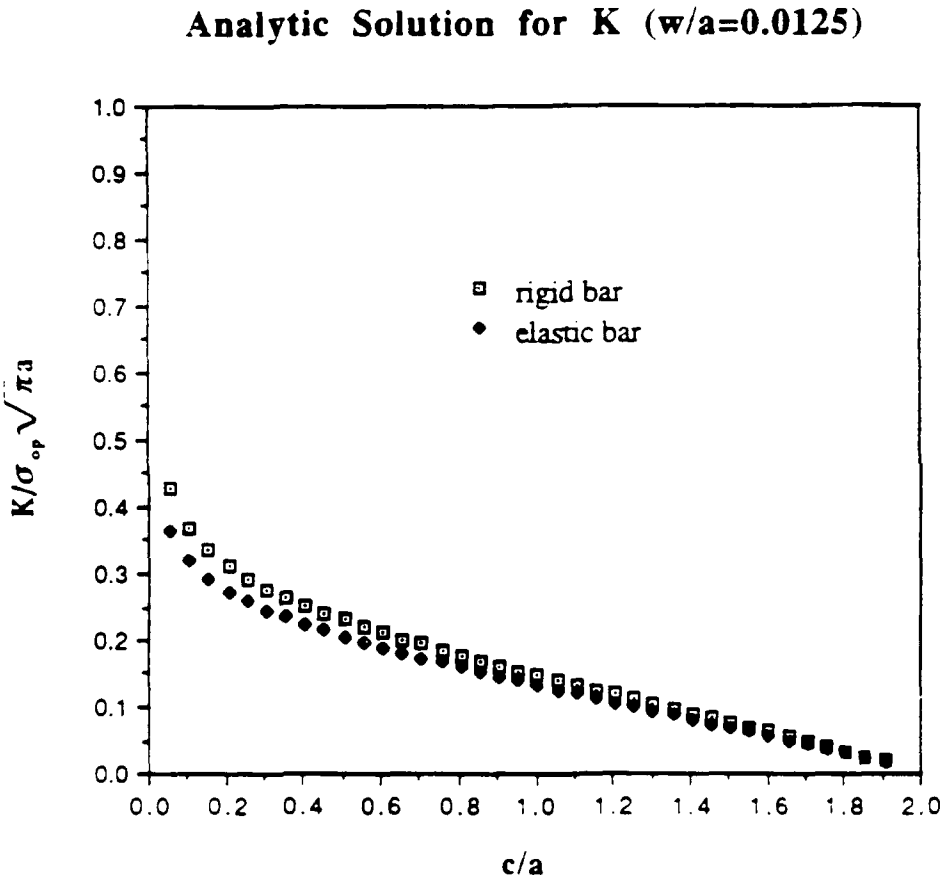

Fig. 13. Variations of K for different asperity locations. The asperity width (w) is fixed and the position (c) varies. Both w and c are normalized with respect to crack length.

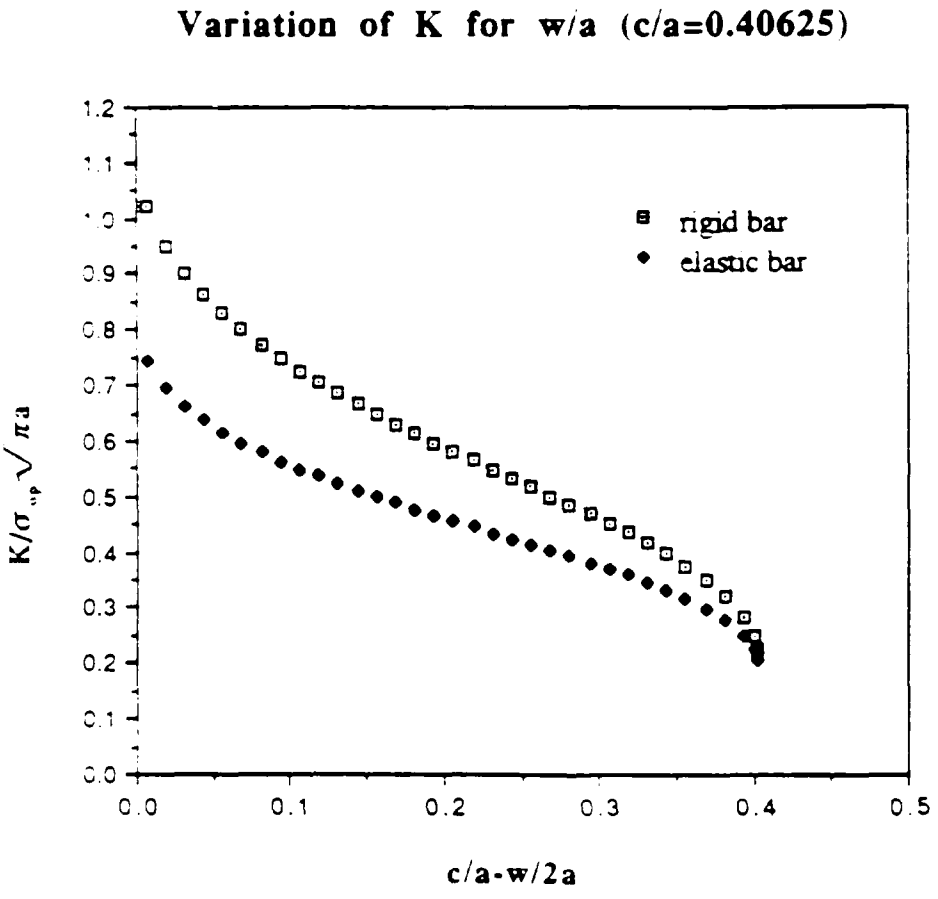

Fig. 14. Variations of K with the asperity width. The position is fixed.

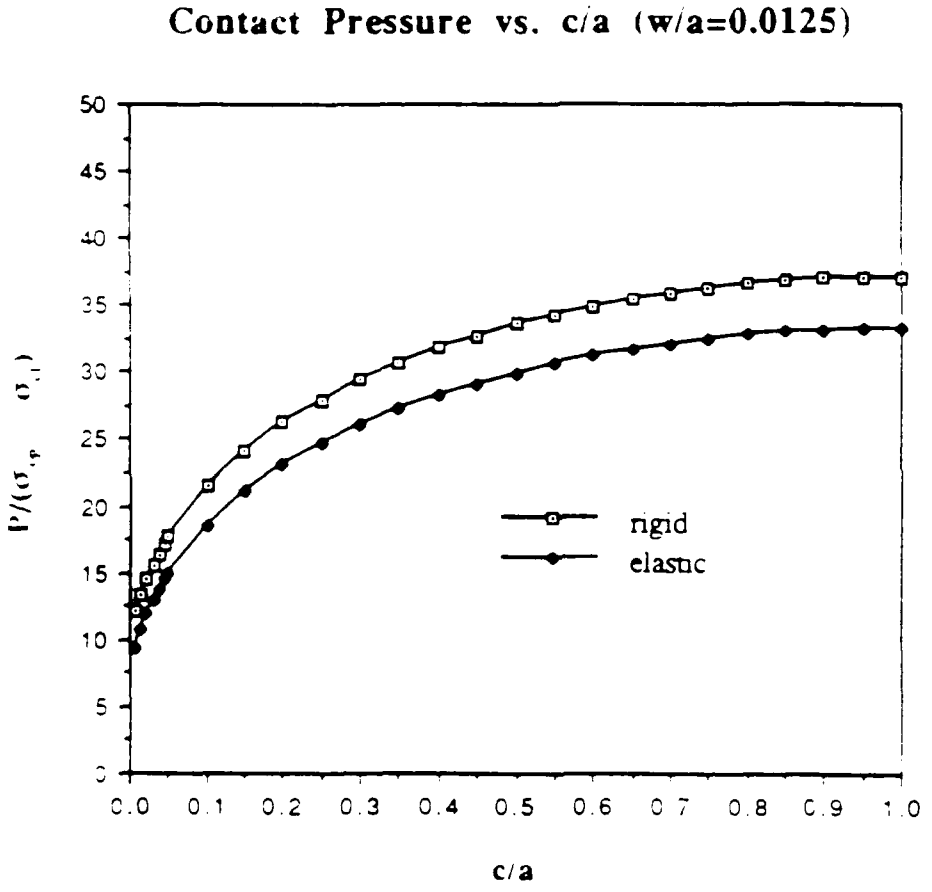

Fig. 15. **Variation of P along the asperity location**

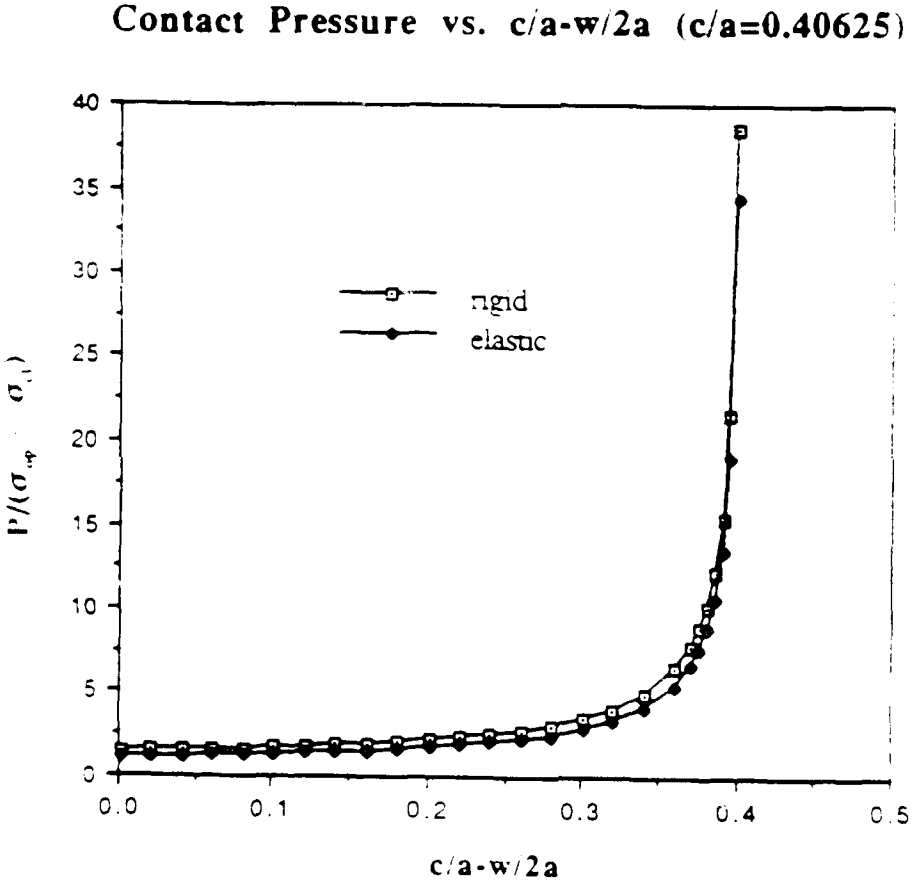

Fig. 16 Variation of P with the asperity width

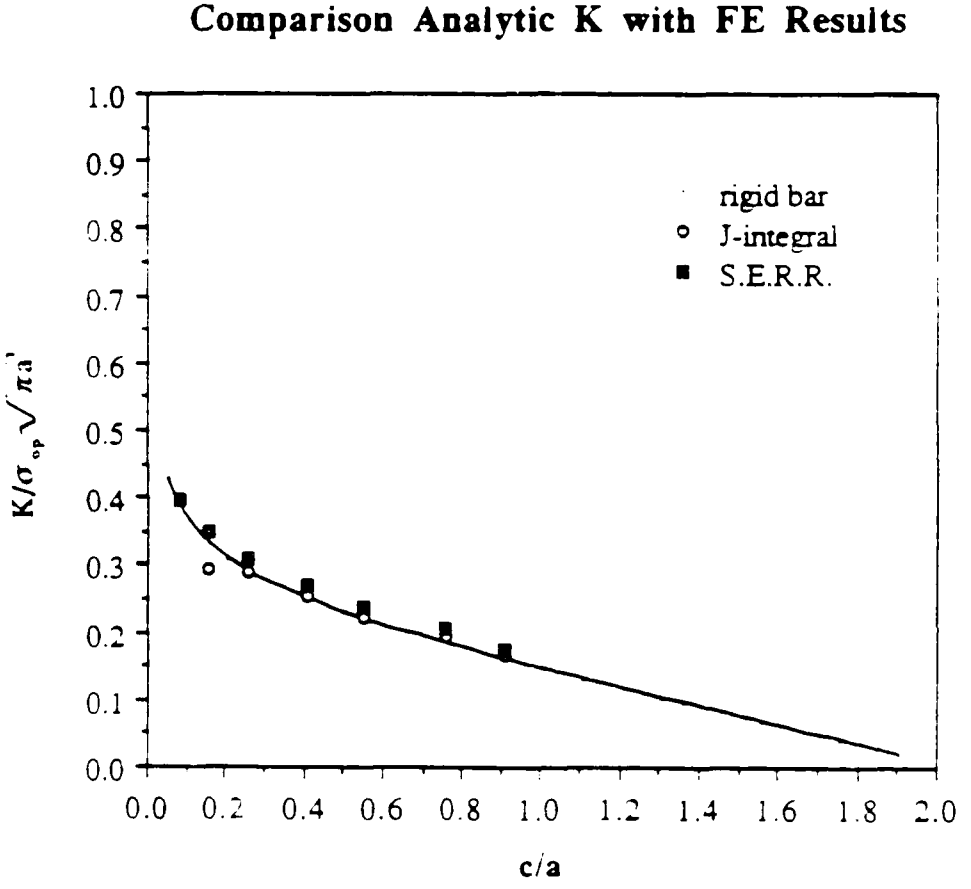

Fig. 17. **Comparison of K for a rigid asperity**

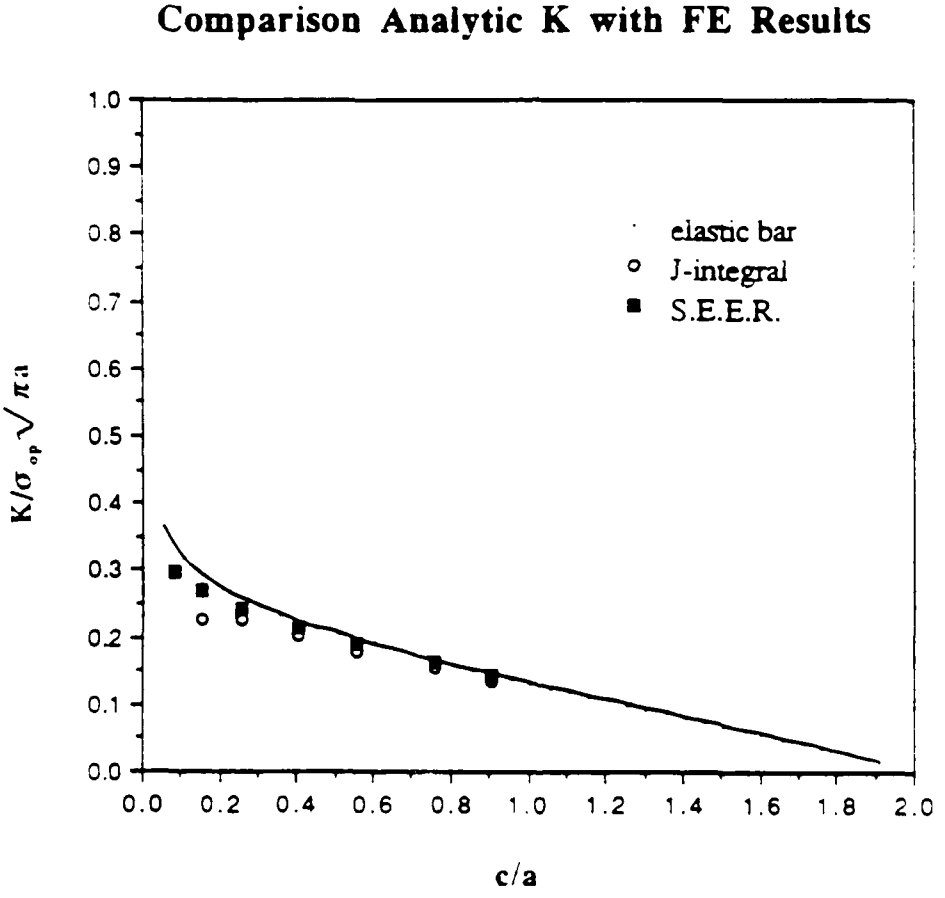

Fig. 18. **Comparison of K for an elastic asperity**

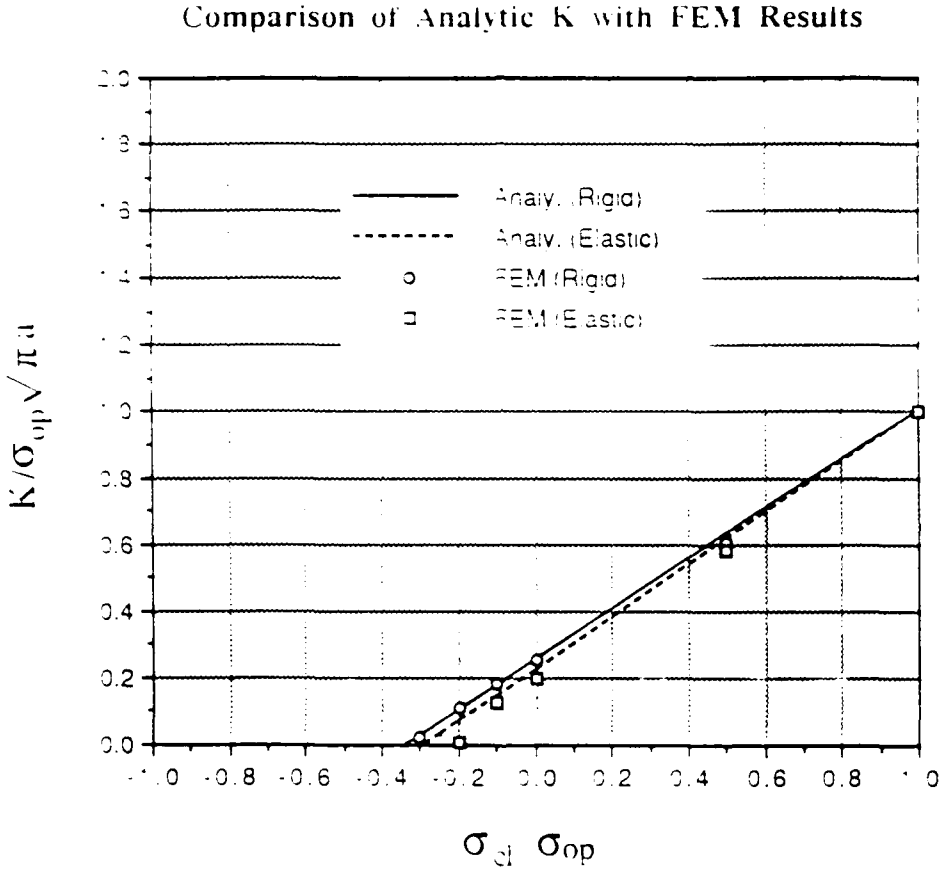

Fig. 19. Comparisons of K for various σ_{cl}/σ_{op}

Metal Matrix Composites", ASTM International Symposium on Damage Defection and Quality Assurance in Composite Materials, November 1990, San Antonio.

5. "Impact of a SiC/Al MMC of X-ray Tomographic Microscopy on Deformation Studies," (presented by T.M. Breunig) Fall 1990 Materials Research Society Symposium on Advanced Tomographic Imaging Methods for the Analysis of Materials, November 1990, Boston.

Publication

"A Framework Relating Macroscopic Measures and Physical Processes of Crack Closure of Al-Li Alloy 2090," T.M. Breunig, S.R. Stock, S.D. Antolovich, J.H. Kinney, W.N. Massey and M.C. Nichols, to appear in 22nd National Symposium on Fracture Mechanics, 1990.

IX. Trade journals articles (written by the journal's staff) mentioning the in situ load frame and the XTM results.

Aerospace America, Feb. 1991, Designer's Notebook, pp.44-45.
Ceramic Bulletin, Feb. 1991, **70**, p. 203.
Metalworking News, June 18, 1990, pp. 6,20.

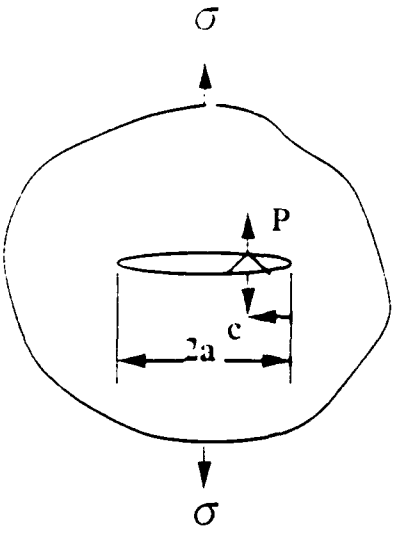

Fig. 4. Asperity in an infinite body

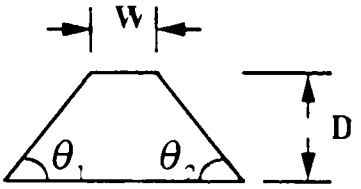

Fig. 5 Asperity Dimension

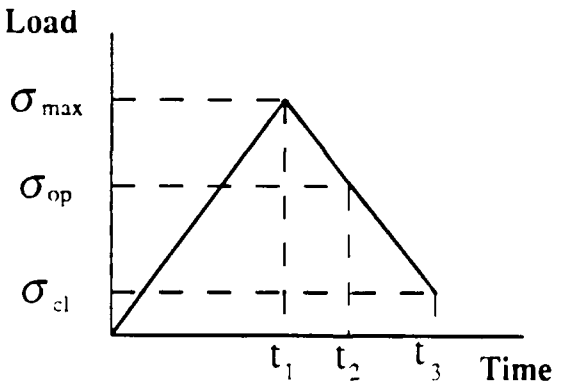

Fig. 6. Loading Scheme

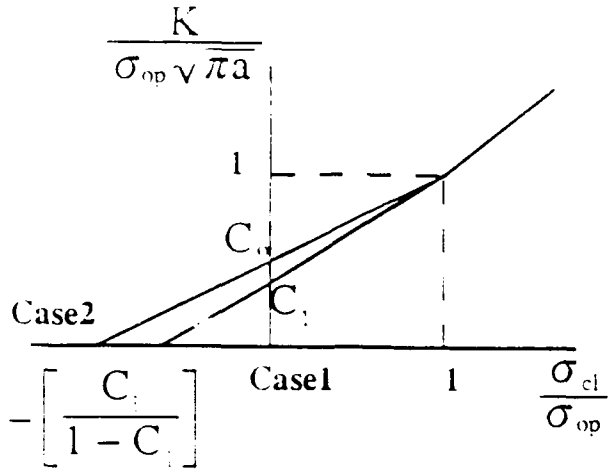

Fig 7. Graphical representation of K

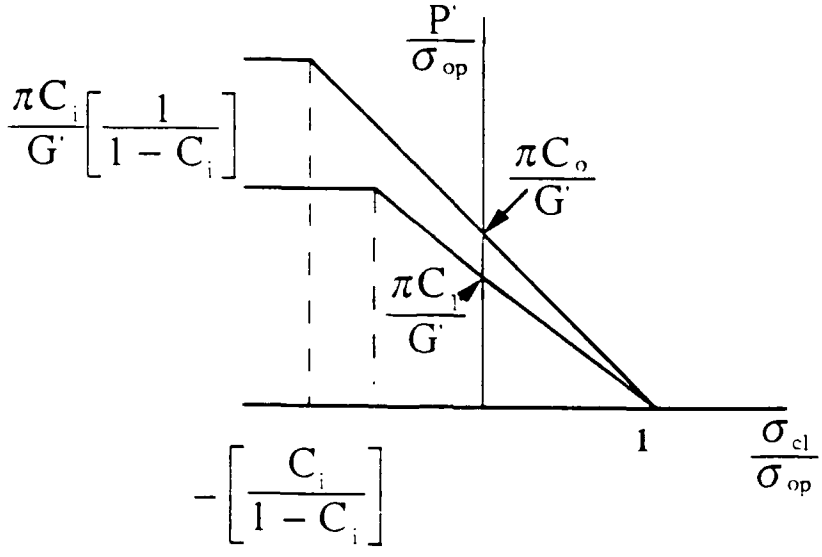

Fig. 8. P as a function of σ_{cl}/σ_{op}

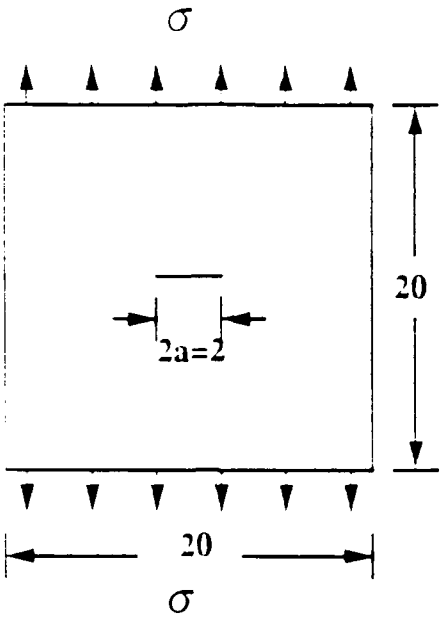

Fig. 9. Specimen Geometry

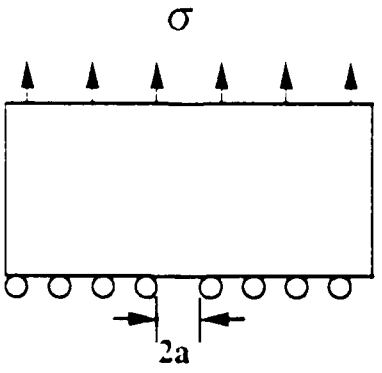

Fig. 10. Half Model

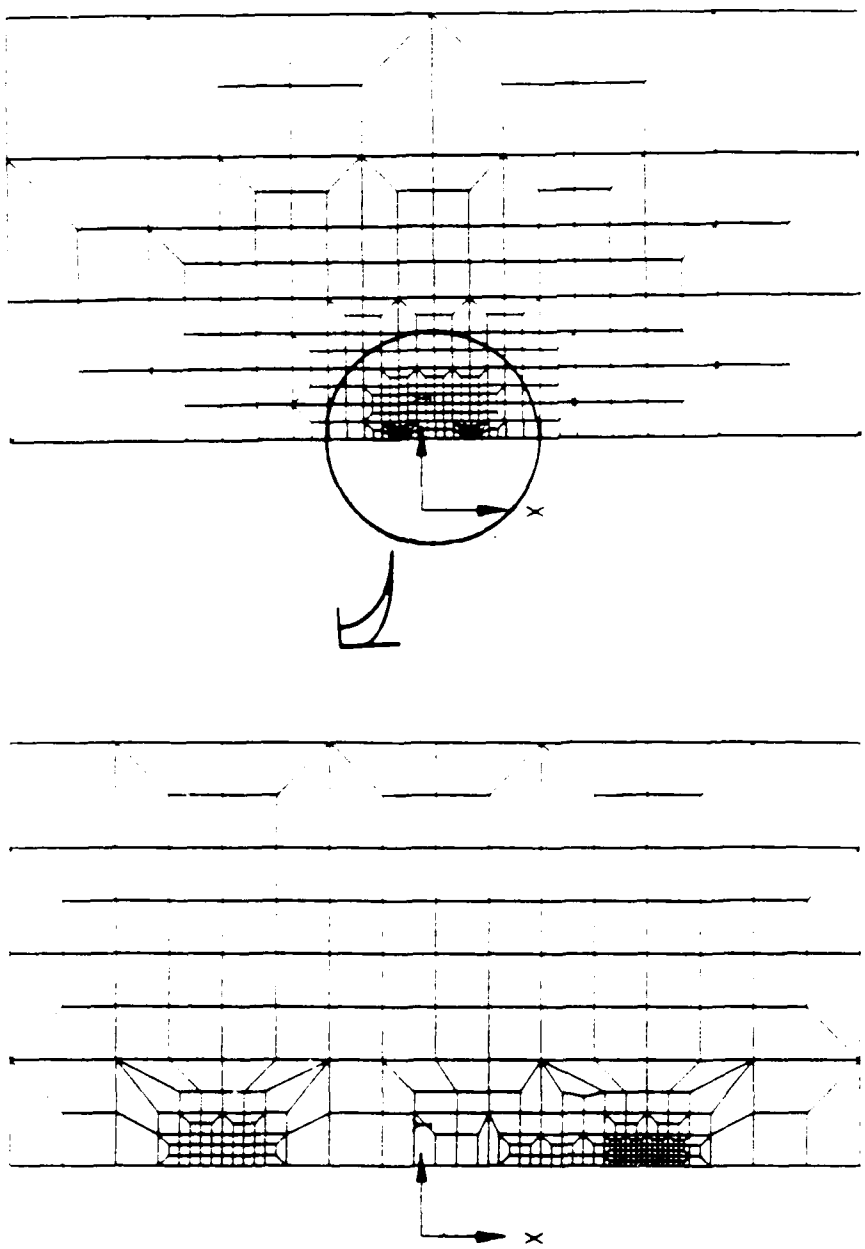

Fig. 11. Finite Element Mesh for a Rigid Asperity

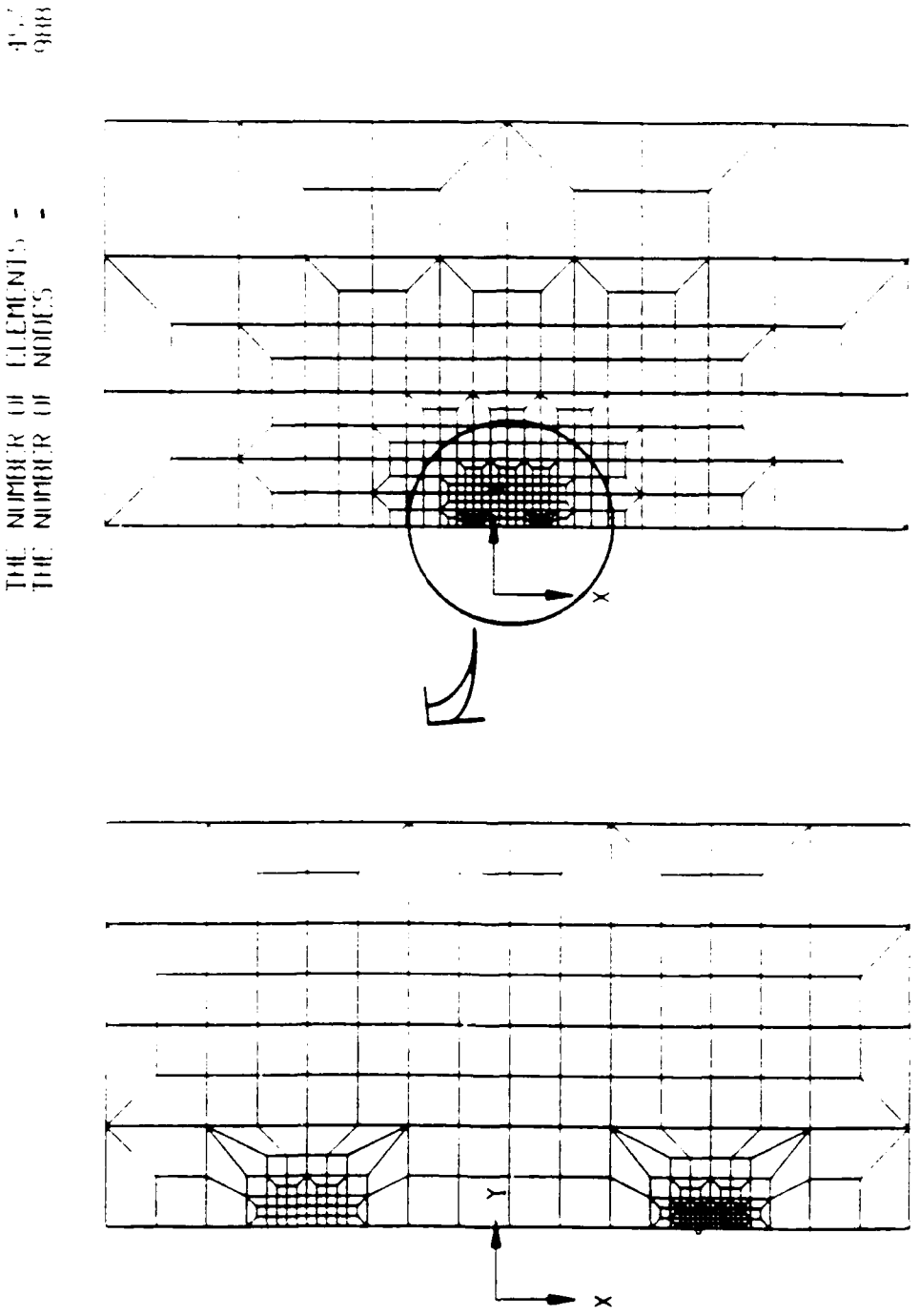

Fig. 12. **Finite Element Mesh for an Elastic Asperity**

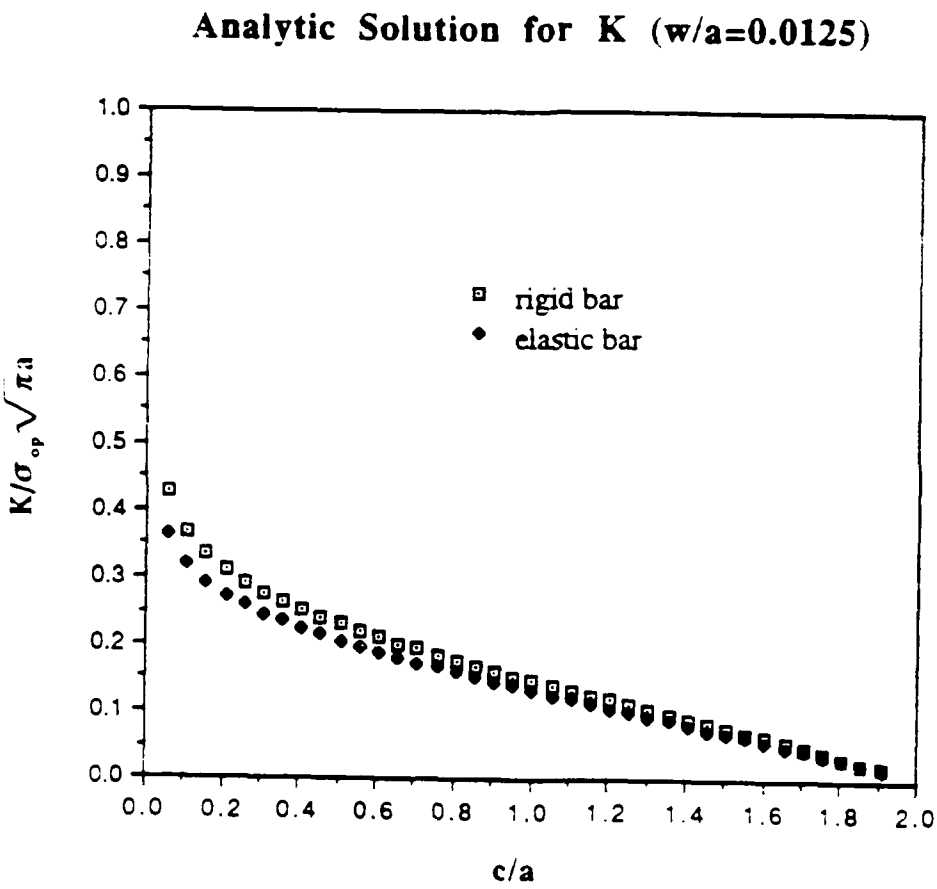

Fig. 13. Variations of K for different asperity locations. The asperity width (w) is fixed and the position (c) varies. Both w and c are normalized with respect to crack length.

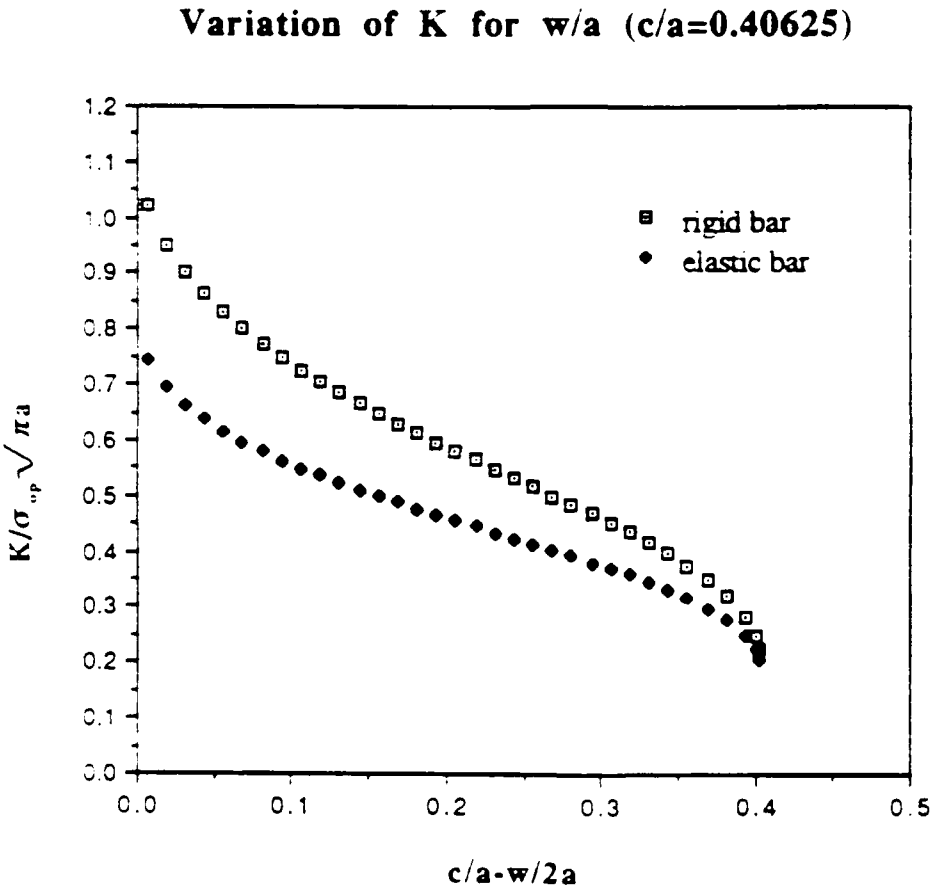

Fig. 14. Variations of K with the asperity width. The position is fixed.

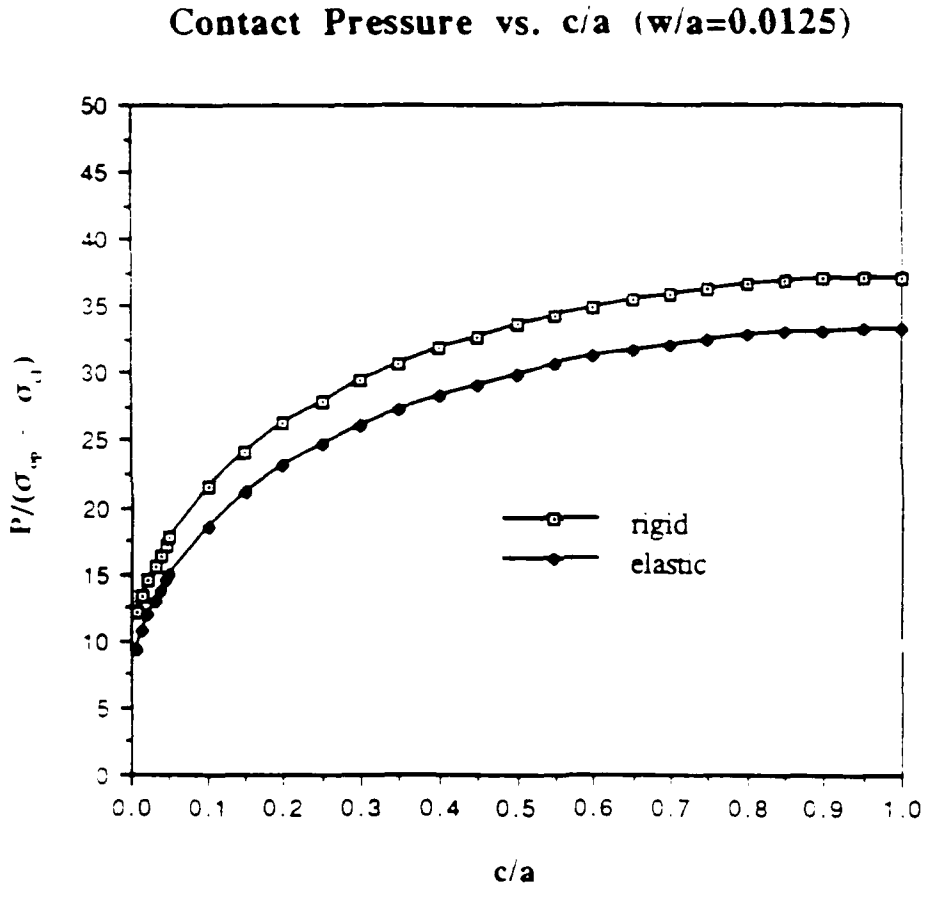

Fig. 15. **Variation of P along the asperity location**

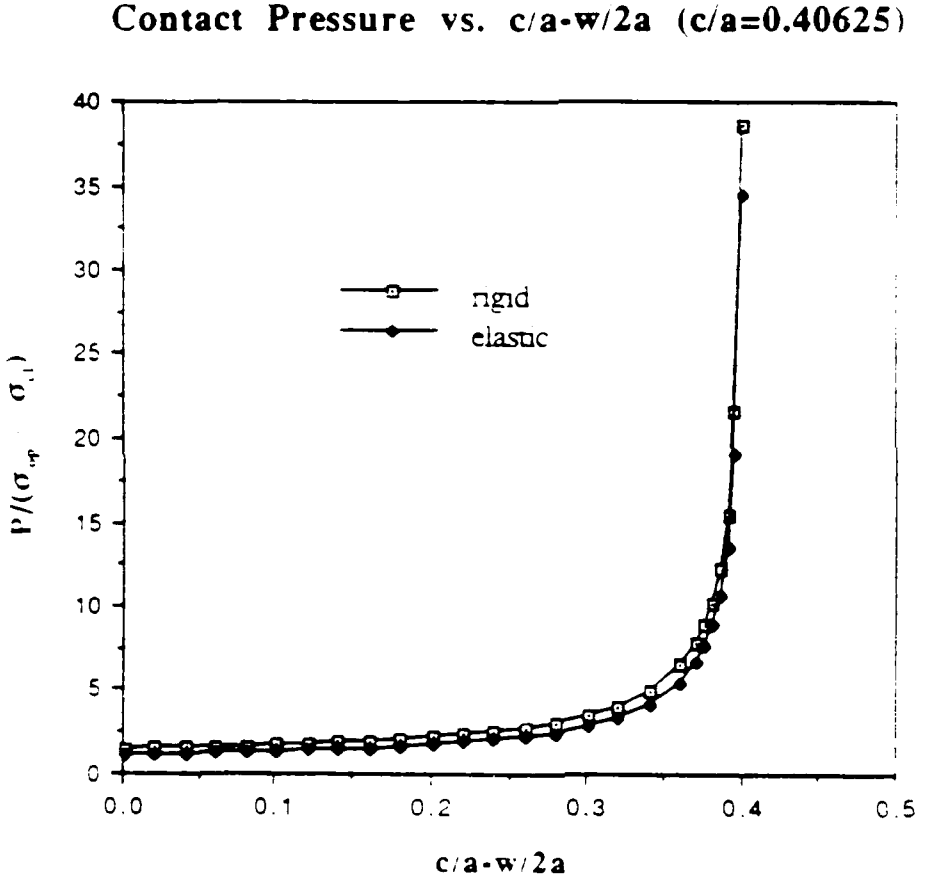

Fig. 16 **Variation of P with the asperity width**

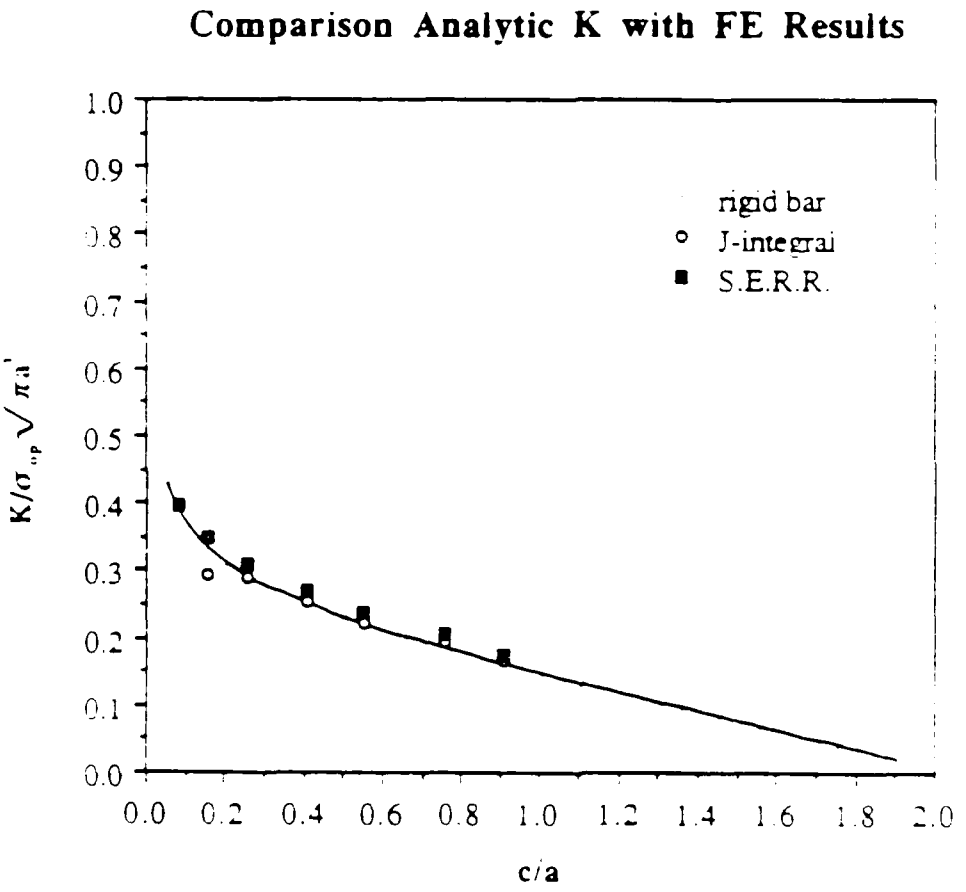

Fig. 17. **Comparison of K for a rigid asperity**

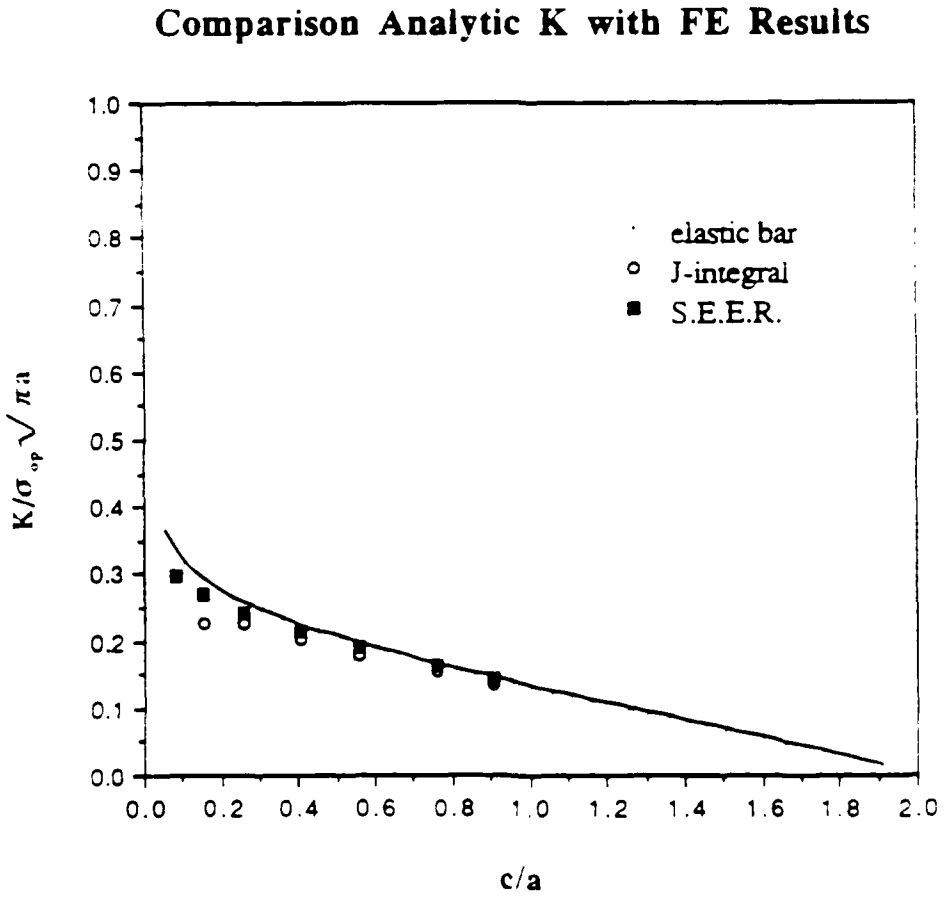

Fig. 18. **Comparison of K for an elastic asperity**

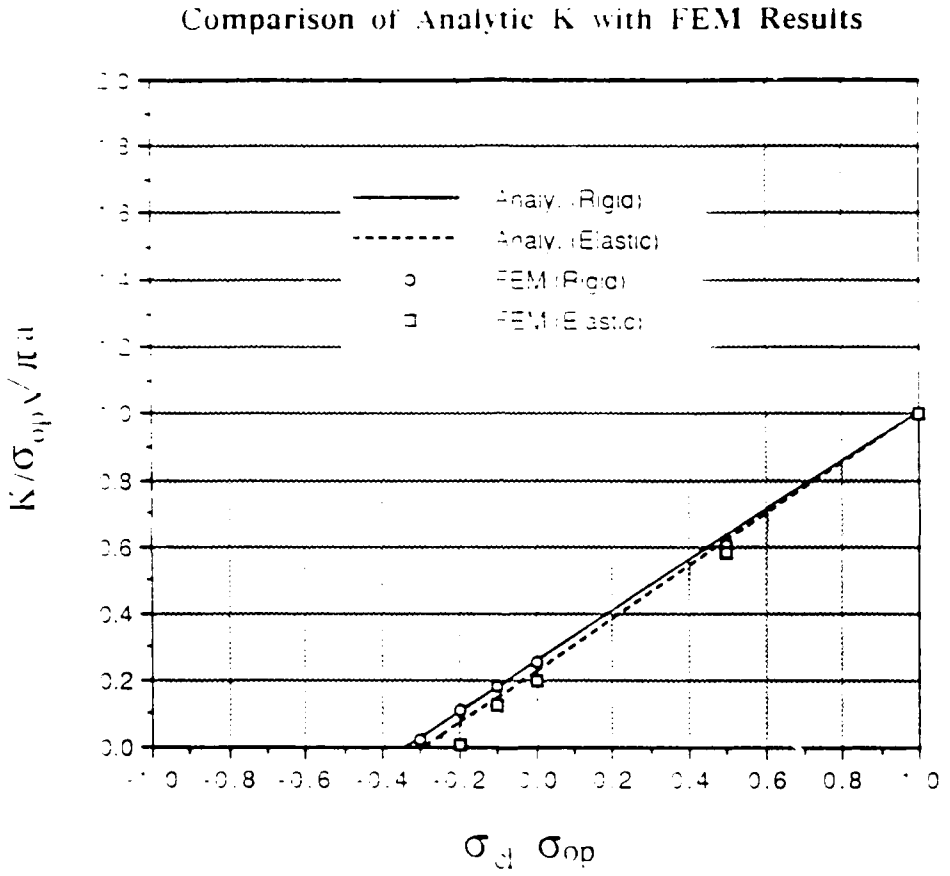

Fig. 19. Comparisons of K for various σ_{cl} σ_{op}